SCIENTIFIC REPORTS

OPEN

CONFERENCE PROCEEDINGS

ACSMS2014

SUBJECT AREAS:
PHOTOCATALYSIS
RENEWABLE ENERGY

Received
4 August 2014

Accepted
29 September 2014

Published
15 October 2014

Correspondence and requests for materials should be addressed to S.S. (shshen_xjtu@mail.xjtu.edu.cn) or S.S.M. (ssmao@me.berkeley.edu)

Surface Engineered Doping of Hematite Nanorod Arrays for Improved Photoelectrochemical Water Splitting

Shaohua Shen[1,2], Jigang Zhou[3], Chung-Li Dong[4], Yongfeng Hu[3], Eric Nestor Tseng[4], Penghui Guo[1], Liejin Guo[1] & Samuel S. Mao[2]

[1]International Research Center for Renewable Energy, State Key Laboratory of Multiphase Flow in Power Engineering, Xi'an Jiaotong University, Shaanxi 710049, China, [2]Department of Mechanical Engineering, University of California at Berkeley, Berkeley, CA 94720, United States, [3]Canadian Light Sources Inc., 44 Innovation Boulevard, Saskatoon, S7N2V3, Canada, [4]National Synchrotron Radiation Research Center, 101 Hsin-Ann Road, Hsinchu Science Park, Hsinchu 30076, Taiwan, China.

Given the narrow band gap enabling excellent optical absorption, increased charge carrier density and accelerated surface oxidation reaction kinetics become the key points for improved photoelectrochemical performances for water splitting over hematite (α-Fe_2O_3) photoanodes. In this study, a facile and inexpensive method was demonstrated to develop core/shell structured α-Fe_2O_3 nanorod arrays. A thin, Ag-doped overlayer of ~2–3 nm thickness was formed along α-Fe_2O_3 nanorods via ultrasonication treatment of solution-based β-FeOOH nanorods in Ag precursor solution followed by high temperature annealing. The obtained α-Fe_2O_3/$Ag_xFe_{2-x}O_3$ core/shell nanorod films demonstrated much higher photoelectrochemical performances as photoanodes than the pristine α-Fe_2O_3 nanorod film, especially in the visible light region; the incident photon-to-current efficiency (IPCE) at 400 nm was increased from 2.2% to 8.4% at 1.23 V *vs.* RHE (Reversible hydrogen electrode). Mott-Schottky analysis and X-ray absorption spectra revealed that the Ag-doped overlayer not only increased the carrier density in the near-surface region but also accelerated the surface oxidation reaction kinetics, synergistically contributing to the improved photoelectrochemical performances. These findings provide guidance for the design and optimization of nanostructured photoelectrodes for efficient solar water splitting.

Hematite (α-Fe_2O_3), commonly known as "rust", has emerged as a promising candidate for photoelectrochemical (PEC) water splitting due to its favorable physicochemical properties of narrow band gap (2.1–2.2 eV), chemical stability, nontoxicity, abundance, and low cost[1–4]. However, inherent limitations such as short hole diffusion length (2–4 nm), high charge recombination rate, and slow oxygen evolution reaction kinetics[5–7] inhibit the PEC performances of α-Fe_2O_3 photoanodes. As such, given the narrow band gap enabling excellent optical absorption, increased charge carrier density and accelerated surface oxidation reaction kinetics become the key points for improved photoelectrochemical performances for α-Fe_2O_3 photoanodes.

Metal ion doping, as an effective way to promote charge transfer by increasing donor density and improving the electronic conductivity of α-Fe_2O_3, has attracted enormous efforts with a number of metal ions (Ti, Zr, Sn, Pt, *etc.*) as dopants[1]. For instance, Wang *et al.* reported that Ti-doped α-Fe_2O_3 prepared by a facile deposition-annealing process showed greatly enhanced PEC performance due to the increased donor density and reduced electron-hole recombination at the time scale beyond a few picoseconds[8]. Zr doping was also found to enhance the PEC performance of α-Fe_2O_3 nanorod arrays by reducing the rate of electron–hole recombination[9].

Slow water oxidation reaction kinetics, another main factor limiting the PEC water splitting effciency of α-Fe_2O_3 as photoanodes, was previously found to be effectively improved by surface treatment[10]. A thin overlayer of metal oxides such as Al_2O_3, Ga_2O_3, In_2O_3, and ZnO, has been demonstrated to effectively accelerate solar water oxidation by passivating surface states of α-Fe_2O_3[11–13]. The kinetics can be also improved by modifying the α-Fe_2O_3 surface with specific cocatalysts (*e.g.*, IrO_2, Co_3O_4, Co-Pi, $Ni(OH)_2$) in order to facilitate the four-electron process of water oxidation. This modification generally catalyzes hole transfer and results in suppressed surface charge recombination[14–17]. Recently, a Pt-doped α-Fe_2O_3 nanorod photoanode was reported to show a record-breaking performance of 4.32 mA cm^{-2} PEC water oxidation current at 1.23 V vs. RHE under simulated 1-sun irradiation when an oxygen-evolving Co-Pi cocatalyst was added on the surface[18]. Surface doping of metal ions has proven to be an alternative way to achieve enhanced PEC performances of α-Fe_2O_3 photoanodes by pro-

moting charge migration and/or creating a doped overlayer to catalyze the surface water oxidation reaction[19–22]. Xi *et al.* reported photocurrent improvement in α-Fe_2O_3 nanorod arrays treated by surface Sn doping, which was mainly attributed to a reduced electron–hole recombination at the hematite–electrolyte interface through the formation of an $Fe_xSn_{1-x}O_4$ layer[23]. An α-Fe_2O_3 nanotube photoanode with a thin $Ni_xFe_{2-x}O_3$ overlayer on the surface showed a ~280% enhancement of the photoconversion efficiency relative to the pristine α-Fe_2O_3 nanotube photoanode. This enhancement was indudced by the $Ni_xFe_{2-x}O_3$ overlayer and was attributed to the promoted charge migration, accelerated surface oxygen evolution, and inhibited low-energy photoexcited hole recombination at the semiconductor−liquid junction[24].

As discussed above, increased charge carrier density and accelerated surface oxidation reaction kinetics can be achieved by metal ion doping and surface treatment (cocatalyst decoration or surface doping), respectively. Then, is it possible to reduce the bulk and surface charge carrier recombination by synergistically increasing the charge carrier density and accelerating the surface oxidative reaction kinetics, for efficient solar water splitting over α-Fe_2O_3 photoanodes? In this study, an Ag-doped overlayer was proposed and created on the surface of α-Fe_2O_3 nanorods for improved PEC performances. It was revealed that Ag doping greatly increased the charge carrier density in the near-surface region of α-Fe_2O_3 nanorods, meanwhile the Ag-doped overlayer effectively catalyzed surface oxidation reaction.

Results

Fabrication of α-Fe_2O_3 nanorod arrays with an Ag-doped overlayer. α-Fe_2O_3 nanorod arrays with an Ag-doped overlayer (*i.e.*, Ag-doped α-Fe_2O_3 nanorod films) were developed as photoanodes by a simple and inexpensive method for efficient solar water splitting. Fig. 1 shows the procedure for the Ag-doped α-Fe_2O_3 nanorod films. First, β-FeOOH nanorod arrays were grown on FTO subsrates *via* a solution-based purpose-built method (Step I)[25], and then treated by ultrasonication in an Ag^+ (silver acetate, AgAc) aqueous solution (Step II). The Ag^+-absorbed β-FeOOH nanorod arrays were further annealed at 750°C for 5 min to form Ag-doped α-Fe_2O_3 nanorod films with α-Fe_2O_3 in the internal region and Ag-doped α-Fe_2O_3 ($Ag_xFe_{2-x}O_3$) on the surface. Since the films were ultrasonically treated in Ag^+ aqueous solutions with different concentrations (0.005, 0.01, 0.05, and 0.1 M), the obtained Ag-doped α-Fe_2O_3 nanorod films were designated as Ag/Fe-*n*, where $n = 0.005, 0.01, 0.05, 0.1$, respectively. The crystal structure of these Ag-doped α-Fe_2O_3 nanorod films was confirmed by Raman spectroscopy. As shown in Fig. S1 in Supplementary Information, both pristine and Ag-doped α-Fe_2O_3 nanorod films displayed typical Raman bands of hematite[9,19,20], with no other impurity phase observed. The top view SEM images revealed that after ultrasonication treatment in an Ag^+ solution, the Ag-doped nanorod array films retained their original morphology (Fig. S2), with nanorod diameters of 50–100 nm. The absence of additional peaks in the Raman spectra and the unaltered morphology (*e.g.*, nanorod diameter) for the Ag-doped nanorod array films compared to the pristine hematite indicates that the Ag-doped overlayer is very thin.

To further investigate the morphology and architecture of the Ag-doped α-Fe_2O_3 nanorod array films, TEM images were obtained as shown in Fig. 2. Pristine hematite shows the morphology of nanorods as grown in aqueous solution (Fig. 2A). Although shortened nanorods appear in the pictures, they may have originated during the processing of hematite nanorods for TEM scanning. The high-resolution TEM image of pristine hematite (Fig. 2B) reveals the surface of the nanorods to be very clean and smooth. Although nanorod morphology remained almost unchanged upon doping (see SEM images in Fig. S2), something of interest is observed near the surface for the Ag-doped α-Fe_2O_3 nanorods (Ag/Fe-0.005, Fig. 2C). The atomic arrangement is uniform and well-ordered in the internal regions but gradually fades while approaching the surface of the nanorods. This should be due to the incorporation of Ag into the hematite surface structure and the formation of a thin overlayer of amorphous $Ag_xFe_{2-x}O_3$ on the surface as detected by TEM (Fig. 2C). Such a disordered overlayer, identified by the absence of a uniform crystal lattice, was also observed when Ni^{2+} or Sn^{4+} solutions were used to treat hematite nanostructures[23,24]. By varying the concentration of Ag^+ precursor solution from 0.005 M to 0.1 M, the obtained Ag-doped α-Fe_2O_3 nanorods possessed a similar $Ag_xFe_{2-x}O_3$ overlayer, with thickness estimated to be ~2–3 nm (Fig. 2C–F). However, in the case for higher Ag^+ concentrations, observable nanoparticles of Ag_2O present on the surface of the α-Fe_2O_3 nanorods (Ag/Fe-0.05 and Ag/Fe-0.1, Fig. 2E and 2F). These nanoparticles should be formed from superfluous Ag^+ ions absorbed on the surface of the nanorods after annealing.

The chemical compositions of Ag-doped α-Fe_2O_3 nanorod films were studied by XPS, as shown in Fig. S3. For both pristine α-Fe_2O_3 and Ag-doped α-Fe_2O_3 films, the binding energies of Fe $2p_{3/2}$ and Fe $2p_{1/2}$ levels are located *ca.* 711.1 and 724.4 eV (Fig. S3A), respectively, with an energy difference of 13.3 eV, indicating that iron ions mainly exist as Fe^{3+}. After being treated in Ag^+ aqueous solutions, all films display obvious Ag XPS signals with binding energies of the Ag $3d_{5/2}$ and Ag $3d_{3/2}$ levels located at ca. 367.9 and 374.0 eV (Fig. S3B), respectively. Comparison with XPS data from Schön[26] shows very good agreement and indicates that these Ag 3d signals are from Ag^+ ions. When the concentration of Ag^+ aqueous solution is increased

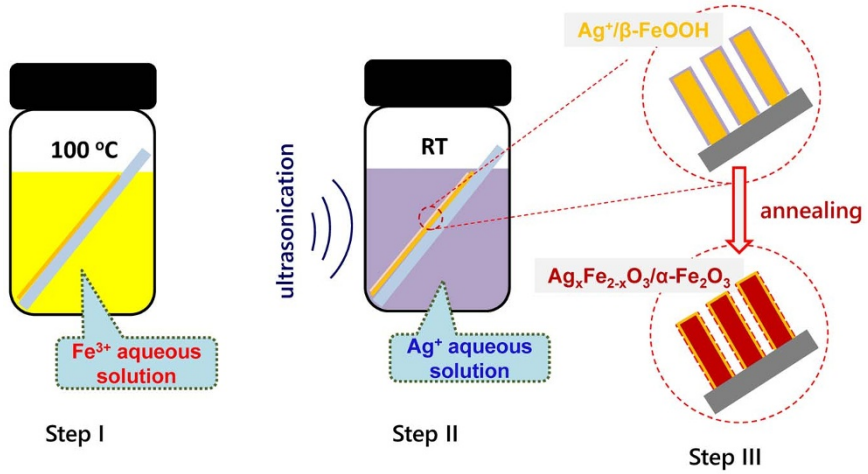

Figure 1 | A schematic showing the preparation of Ag-doped α-Fe_2O_3 nanorod films.

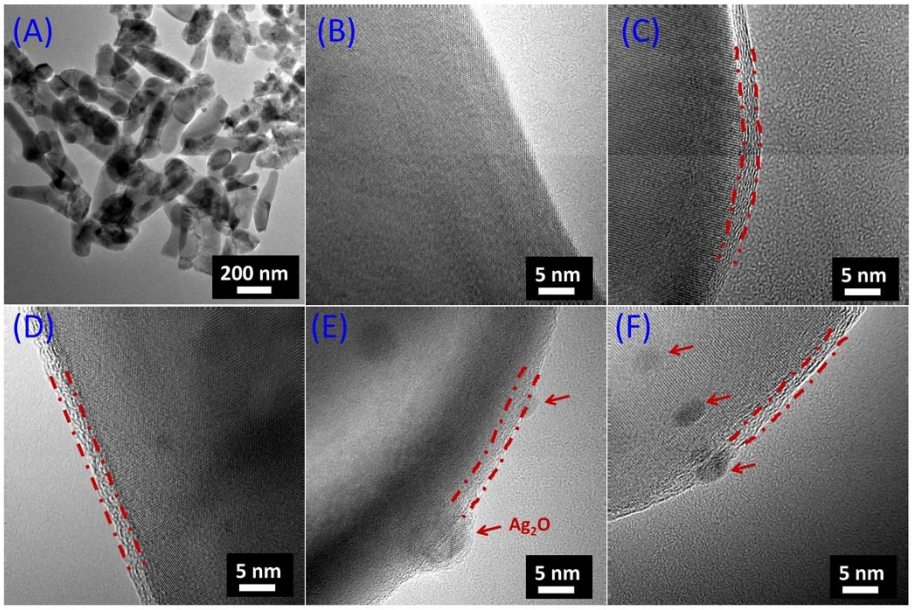

Figure 2 | TEM images of Ag-doped α-Fe_2O_3 nanorod films. (A,B) pristine α-Fe_2O_3, (C) Ag/Fe-0.005, (D) Ag/Fe-0.01, (E) Ag/Fe-0.05, (F) Ag/Fe-0.1.

from 0 to 0.1 M, the surface Ag : Fe molar ratio first increases quickly and then very slowly, as shown in Fig. 3A. This change in the Ag : Fe molar ratio may be explained to some extent by the observations in the TEM images. After being treated in the Ag^+ aqueous solutions, an $Ag_xFe_{2-x}O_3$ overlayer with very similar thickness of 2 ~ 3 nm was formed on all of the Ag-doped α-Fe_2O_3 nanorod films. In short, both surface concentration of Ag^+ and thickness of Ag-doped overlayer are very similar, which may be related to the depth-limited diffusion of surface absorbed Ag^+ ions into the lattice of α-Fe_2O_3 nanorods. Additional nanoparticles, which is likely assigned to Ag_2O due to the absence of metallic Ag XPS signal (Fig. S3B), existed on the surface of the α-Fe_2O_3 nanorods made from the Ag^+ solutions with higher concentration, resulting in the slightly increased Ag : Fe molar ratio for the surfaces of these nanorods. The Sn XPS signal originates from Sn^{4+} ions that diffused from FTO to α-Fe_2O_3 during high temperature annealing (Fig. S3C)[27,28]. It is generally accepted that the PEC properties of α-Fe_2O_3 depend on the concentration of Sn^{4+} very sensitively[27,28]. In the present study, both pristine and Ag-doped α-Fe_2O_3 nanorod films underwent the same annealing process (annealed at 750°C for 5 min), providing the very similar condition for Sn^{4+} diffusion in α-Fe_2O_3 nanorods. Thus, the resulted similar and very low Sn^{4+} concentrations (Sn : Fe molar ratio: 0.034 ~ 0.045) in these pristine and Ag-doped α-Fe_2O_3 nanorod films should be not the main reason for their varied PEC performances. In Fig. S3D, the binding energies of the O 1s levels for both pristine and Ag-doped α-Fe_2O_3 nanorod films are very similar to those for hematite in the literature[23,29].

The depth distribution of Ag in the Ag-doped α-Fe_2O_3 nanorod films was examined by an XPS Ar^+ etching measurement. XPS measurements were conducted during controlled Ar^+ etching from 0 to 1100 s, taking the Ag/Fe-0.05 film as the representative sample. As shown in Fig. S4, the peak areas of Fe 2p (Fig. S4A) and O 1s (Fig. S4B) unsurprisingly remain almost unchanged upon Ar^+ etching, whereas the peak area of Sn 3d increases (Fig. S4C). This result corresponds to the graded distribution of Sn diffused from the FTO substrate, as shown by the Sn : Fe molar ratio curve in Fig. 3B. One can easily observe that after slightly decreasing at the initial etching stage, the molar ratio of Ag : Fe levels out at ~0.02 (Ag : Fe molar ratio curve in Fig. 3B), which can be also evidenced by the change of peak area of Ag 3d in Fig. S4D. The slightly higher molar ratio of Ag : Fe at the film surface (0 s etching) is reasonable, given

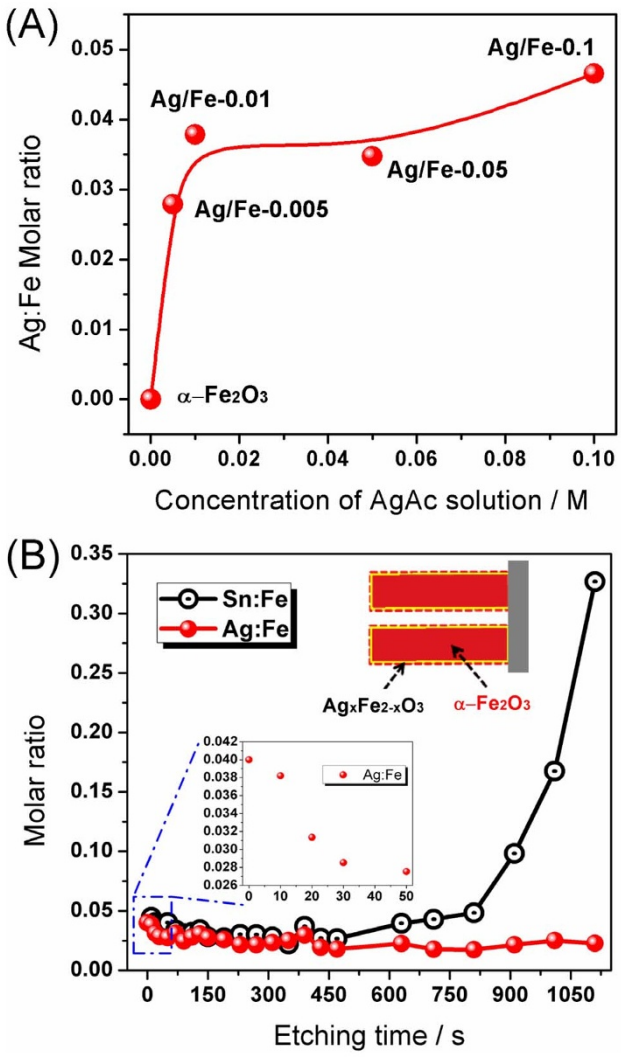

Figure 3 | (A) Molar ratio of Ag : Fe at the surface of Ag-doped α-Fe_2O_3 nanorod films, (B) XPS etching profile of the Ag/Fe-0.05 film.

that the surface of the α-Fe_2O_3 nanorods was covered by the Ag-doped α-Fe_2O_3 overlayer. Finally, the constant molar ratio of Ag : Fe during Ar^+ etching indicates a homogenous distribution of Ag^+ dopants along the α-Fe_2O_3 nanorods. Thus, a uniform and thin overlayer of Ag-doped α-Fe_2O_3 ($Ag_xFe_{2-x}O_3$) formed on the entire surface of the α-Fe_2O_3 nanorods, as previously confirmed in the TEM images. A schematic of the architecture of the Ag-doped α-Fe_2O_3 nanorod films and also the distribution of the Ag-doped overlayer ($Ag_xFe_{2-x}O_3$), based on the TEM images and XPS analysis results, can be seen in the inset of Fig. 3B.

To check the effect of Ag surface doping on the optical absorption property of α-Fe_2O_3, transmittance spectra for pristine and Ag-doped α-Fe_2O_3 nanorod films were recorded (Fig. S5A). It can be seen that both pristine and Ag-doped α-Fe_2O_3 nanorod films have very similar optical transmittance profiles, and all the films are calculated to have similar band gaps of ~2.1 eV by the Kubelka-Munk equation (Fig. S5B)[30]. Thus, the optical properties of these Ag-doped α-Fe_2O_3 nanorod films should not be related to the difference in PEC performances of both pristine and Ag-doped α-Fe_2O_3 nanorod films, as discussed in the following section.

The X-ray absorption spectrum (XAS) technique was used as a sensitive local structure probe[31,32] to clarify the surface structure of α-Fe_2O_3 nanorods after surface doping with Ag^+, and the Fe *L*-edge and O *K*-edge XANES spectra were recorded in surface sensitive total electron yield (TEY) for the pristine and Ag-doped α-Fe_2O_3 nanorod (Ag/Fe-0.05) films. The chemical state of Fe in α-Fe_2O_3 nanorods after surface doping with Ag^+ was investigated by Fe *L*-edge spectra, as shown in Fig. 4A. L_3 and L_2-edges located at ~710 eV and ~721 eV have been assigned to Fe(*2p*) transitions to an unoccupied *3d* orbital. The distinct splitting at L_3-edge remains for both films, with small pre-peak follow by main peak, suggesting presence of only Fe^{3+} valence form[33]. For the Ag-doped α-Fe_2O_3 nanorod (Ag/Fe-0.05) films, the increase in spectral intensity of Fe *L*-edge (Fig. 4A, inset) indicates more unoccupied Fe(*3d*) states[34], which clearly presents the chemical interaction between α-Fe_2O_3 and Ag^+, probably promoting the charge transfer from Fe(*3d*) state to Ag(*3d*) and/or O(*2p*) states due to the orbital mixing. In the normalized O *K*-edge XANES spectra depicted in Fig. 4B, the first feature in the pre-edge region at ~530 eV, split into Fe *3d* t_{2g} and e_g states, should be related to the low energy transition from the O(*1s*) state to the hybridized O(*2p*)−Fe(*3d*) state. The second feature at energies greater than 535 eV corresponds to O(*2p*) state hybridized with Fe(*4s,4p*) states[35]. The first feature of the O *K*-edge spectra has been used to assess the extent of the hybridization of O(*2p*) state with *3d* states of transition metal atoms[36,37]. Suntivich *et al.*[38] proposed that the spectral intensity is linearly proportional to the product of the total number of the empty *2p*−*3d* (oxygen − transition metal) state and their extent of hybridization. Alternatively, the intensity ratio of the O(*2p*)−Fe(*3d*) feature relative to the broad O(*2p*)−Fe(*4s,4p*) feature, can be used to quantify the relative contribution of covalent bonding in α-Fe_2O_3[38]. In the present study, although increase in spectral intensity of the first feature is neglectable, the intensity ratio of the two features (the O(*2p*)−Fe(*3d*) and O(*2p*)−Fe(*4s,4p*) bands) is obviously higher for the Ag-doped sample than the pristine one (0.47 *vs.* 0.42). This indicated the higher extent of O(*2p*)−Fe(*3d*) hybridization for the obtained Ag/Fe-0.05 film. It was believed that the increasing hybridization could lead to increased oxygen electrocatalysis[37], which possibly renders the Ag-doped overlayer to act as water oxidation catalyst to accelerate surface oxidation reaction kinetics and hence benefit the PEC water splitting over Ag-doped α-Fe_2O_3 nanorod films as discussed below.

PEC water splitting activity of Ag-doped α-Fe_2O_3 nanorod films. PEC measurements were performed in a three electrode configuration to evaluate the performances of Ag-doped α-Fe_2O_3 nanorod films as photoanodes for solar water splitting. Fig. 5A–E shows a set of current-potential (I-V) curves under chopped 100 mW·cm^{-2} (AM 1.5G) illumination. Upon illumination, a photocurrent onset was observed at *ca.* −0.2 V, after which the photocurrent nearly linearly increased to ~0.05 mA·cm^{-2} at 1.0 V vs. Ag/AgCl for the pristine α-Fe_2O_3 nanorod film (Fig. 5A). In contrast, after surface doping of Ag^+, the obtained Ag-doped α-Fe_2O_3 nanorod films exhibited greatly improved PEC performances. While examing the photocurrents at a bias of 1.0 V vs. Ag/AgCl, one can find that with increasing Ag^+ concentration in aqueous solution for ultrasonication treatment, the reproducible photocurrents (2–4 anodic I-V scans) increased from ~0.15 mA·cm^{-2} for the Ag/Fe-0.005 film (Fig. 5B) to ~0.18 mA·cm^{-2} for the Ag/Fe-0.01 film (Fig. 5C), and then reached the highest value of ~0.22 mA·cm^{-2} (*i.e.*, 340% improvement, relative to the pristine α-Fe_2O_3 nanorod film) for the Ag/Fe-0.05 film (Fig. 5D). However, further increase in Ag^+ concentration resulted in decreased PEC performance. The Ag/Fe-0.1 film exhibited a photocurrent of ~0.13 mA·cm^{-2} at 1.0 V *vs.* Ag/AgCl (Fig. 5E). By further checking the repeated anodic I-V scans, a strong peak appeared between 0 V and 0.4 V during the first anodic scan for all the Ag-doped α-Fe_2O_3 nanorod films. In the repeated I-V scans, this peak became weaker and weaker and then diminshed after two I-V scans for Ag/Fe-*n* (*n* = 0.005, 0.01) and four I-V scans for Ag/Fe-*n* (*n* = 0.05, 0.1). Considering the anodic oxidation reaction happens at the

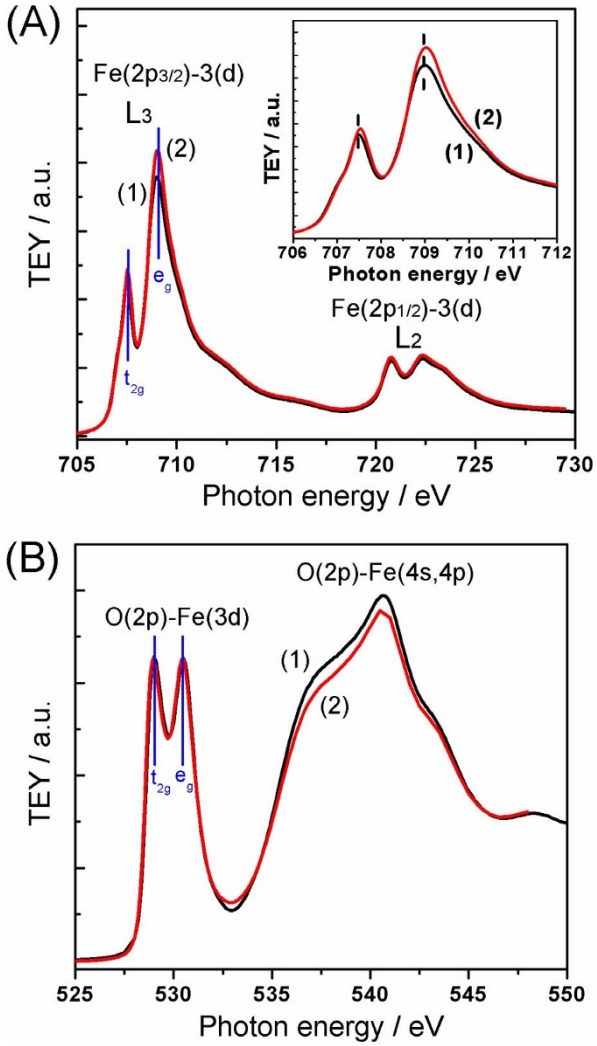

Figure 4 | (A) Fe *L*-edge and (B) O *K*-edge XANES spectra recorded in TEY mode for (1) α-Fe_2O_3 and (2) Ag/Fe-0.05 films.

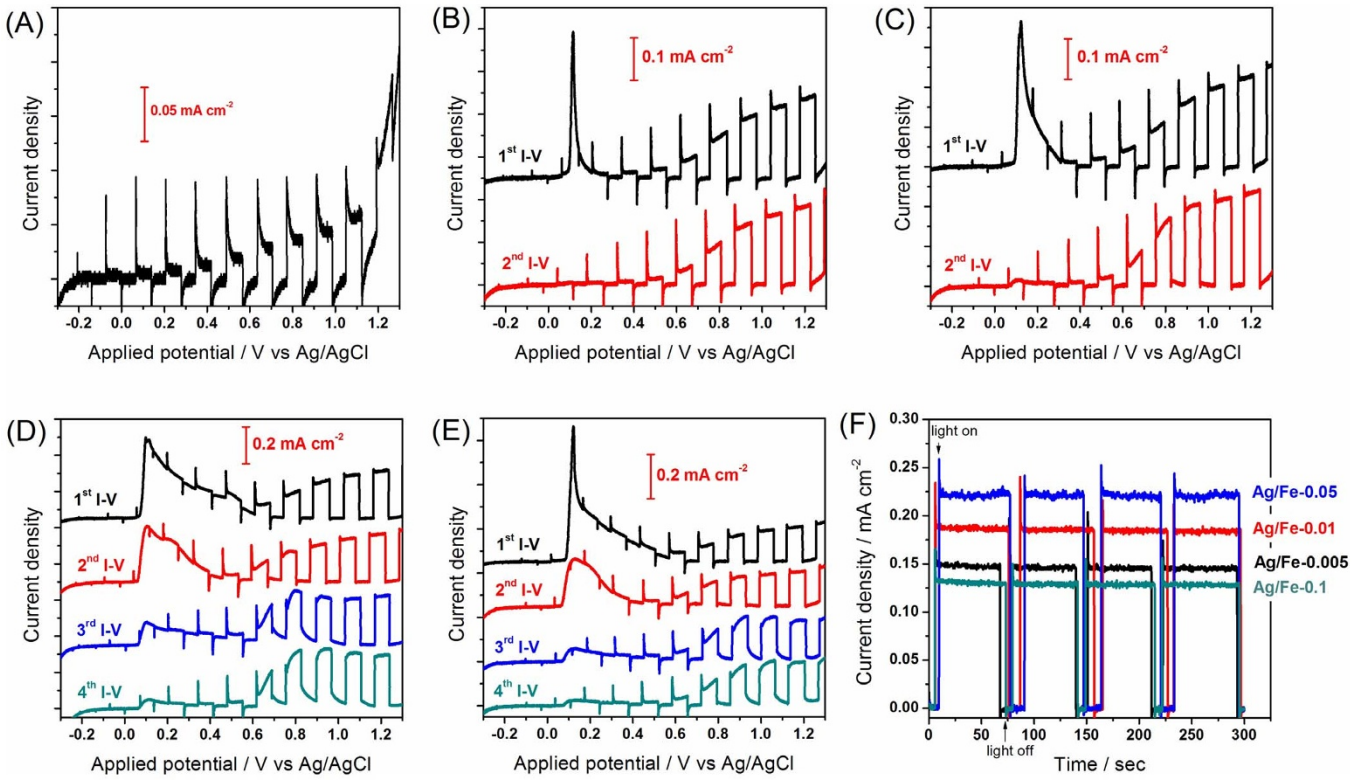

Figure 5 | Photocurrent-potential (I-V) curves of Ag-doped α-Fe_2O_3 nanorod films, (A) pristine α-Fe_2O_3, (B) Ag/Fe-0.005, (C) Ag/Fe-0.01, (D) Ag/Fe-0.05, (E) Ag/Fe-0.1, and (F) Transient photocurrent responses (current density *vs.* time curves) of Ag-doped α-Fe_2O_3 nanorod films at 1.0 V *vs.* Ag/AgCl under simulated solar illumination (AM 1.5G, 100 mW cm^{-2}), following the photocurrent-potential (I-V) measurements shown in Fig. (A–E).

photoanodes, the peak could be associated with the partial oxidation of Ag^+ in the Ag-doped α-Fe_2O_3 nanorod films. To examine this possibility, Ag *3d* XPS spectra measured on the Ag-doped α-Fe_2O_3 nanorod film (Ag/Fe-0.05) before and after the I-V scans were compared. As shown in Fig. S6, before the I-V tests, the legible Ag *3d* XPS signals with binding energies of the Ag $3d_{5/2}$ and Ag $3d_{3/2}$ levels located at *ca.* 367.9 eV and 374.0 eV, respectively, can be undoubtedly assigned to Ag^+. After four I-V anodic scans, a small shift to lower binding energies was found for the Ag *3d* XPS signals. Such a decrease in *3d* electron binding energy is unique for Ag in the metal-oxygen systems, where the oxidation number of the metal increases[26]. Moreover, the full-width half-maximum (FWHM) for the Ag $3d_{5/2}$ and Ag $3d_{3/2}$ signals increased from 1.05 eV and 0.97 eV to 1.51 eV and 1.45 eV, respectively. This can be explained by the presence of chemically disparate Ag atoms (*i.e.*, two kinds of silver atoms, Ag^I and Ag^{III}) after I-V anodic scans, since the Ag *3d* signals from AgO ($Ag^IAg^{III}O_2$) are broader than those from Ag_2O ($Ag^I{}_2O$)[26]. Thus, the shift to lower energy and broadened width of the Ag *3d* XPS binding energy signals provides convincing evidence that the oxidation number of Ag ions increases (*i.e.*, Ag^+ is partially oxidized) in Ag-doped α-Fe_2O_3 nanorod films after anodic I-V scans.

To eliminate any skepticism as to the PEC stability of the Ag-doped α-Fe_2O_3 nanorod films, which may spawn from the chemical state change of Ag dopants during I-V measurement, the transient photocurrent response of the Ag-doped α-Fe_2O_3 nanorod films were tested after I-V anodic scans (with no obvious Ag^+ oxidation peak). As shown in Fig. 5F, all Ag-doped α-Fe_2O_3 nanorod films exhibited very stable photocurrents during the entire measurement period, with current retentions reaching almost 100%. Again, one can confirm that the PEC activity of α-Fe_2O_3 nanorod films may be greatly enhanced by surface doping of Ag ions. This is therefore indicative of the positive effects of the $Ag_xFe_{2-x}O_3$ ultrathin overlayer, which is believed to be the major contributing factor for the pronounced photocurrent improvement.

The improvement in PEC activity induced by Ag surface doping was further verified by investigating the incident photon-to-current efficiency (IPCE) at 1.23 V *vs.* RHE as a function of incident light wavelength (Fig. 6). In comparison to the pristine α-Fe_2O_3 nanorod film, the Ag/Fe-0.05 film showed substantially enhanced IPCE values over the entire wavelength range of 300–600 nm. Most notably, the

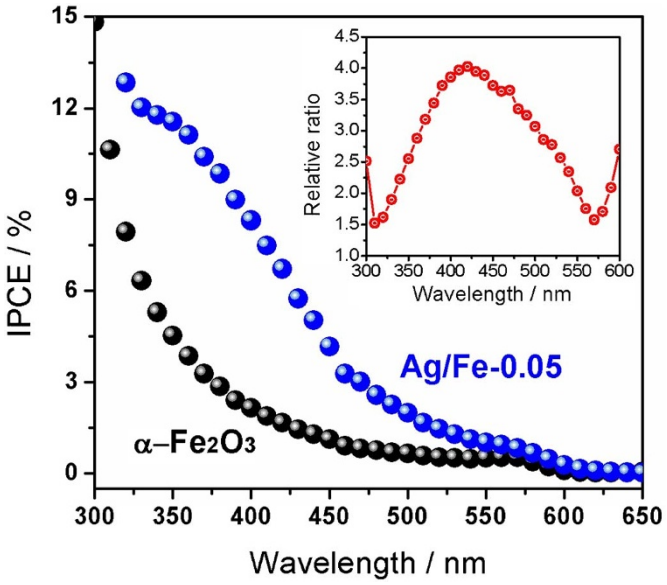

Figure 6 | IPCE of α-Fe_2O_3 and Ag/Fe-0.05 films as photoanodes at 0.65 V *vs.* Ag/AgCl (1.23 V *vs.* RHE). The inset plot shows relative ratio of IPCE of Ag/Fe-0.05 *vs.* α-Fe_2O_3 films.

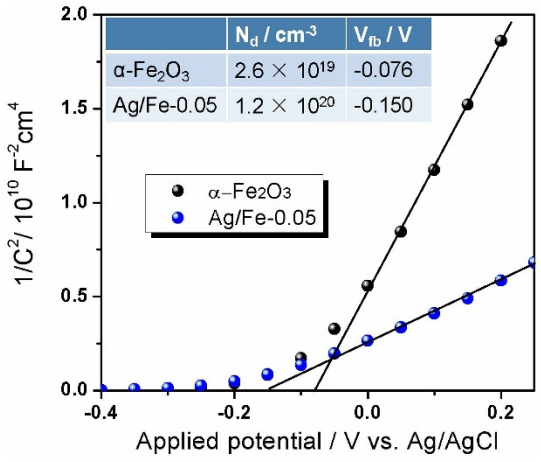

Figure 7 | Mott–Schottky plots of the pristine and Ag-doped Fe_2O_3 nanorod film (Ag/Fe-0.05), inset shows the donor density (N_d) and the flatband potential (V_{fb}).

IPCE value at 400 nm increased from 2.2% to 8.4% after the surface doping. At wavelengths longer than 600 nm, the IPCE value drops to zero, in accordance with the band gap of α-Fe_2O_3[20]. Furthermore, one may also note that the relative ratio of IPCE increase in the visible light region is higher than that of the ultraviolet (UV) region; a ratio of ~4.0 IPCE increase is observed at 400–450 nm (inset of Fig. 6) while a ratio of only ~2.3 IPCE increase is observed at 360 nm. These results are more distinct than those of previous studies in which doping of Ti, Zr, and Sn greatly increased the IPCEs of α-Fe_2O_3 in the UV region while having weaker influence in the visible light region[9,39,40]. However, the intense increase of IPCE in the visible light region was also achieved in a previous study investigating α-Fe_2O_3/$Ni_xFe_{2-x}O_3$ nanotubes as photoanodes. The increase was attributed to greater carrier migration ability as well as the advantageous utilization of carriers at low energy induced by surface doping of Ni into α-Fe_2O_3 nanotubes[24]. Although the PEC activities of these Ag-doped α-Fe_2O_3 nanorod films are still not very high, related to the α-Fe_2O_3 films modified with other electrocatalysts (*e.g.*, IrO_2, Co-Pi, CoO_x and Co_3O_4)[1,14–16], the intense increase in PEC performances especially in visible light region induced by the Ag-doped overlayer is very encouraging.

Discussion

Considering the very similar optical and morphological properties for both pristine and Ag-doped α-Fe_2O_3 nanorod films, doping-induced change in intrinsic electronic properties should mainly contribute to the remarkable improvement in PEC performance for these Ag-doped α-Fe_2O_3 nanorod films acting as water splitting photoanodes. In order to elucidate the effects of Ag surface doping on the electronic properties of α-Fe_2O_3 and hence the enhanced PEC performance, Mott–Schottky (M–S) measurements were carried out in the dark with 1 kHz frequency for the pristine α-Fe_2O_3 and Ag-doped α-Fe_2O_3 (Ag/Fe-0.05) nanorod films. As shown in Fig. 7, both the films showed positive slopes, which indicates that both pristine and Ag-doped samples are n-type semiconductors with electrons as the majority carriers. The smaller slope for the Ag-doped sample reflects a higher electron donor density. The slope in the quasi-linear regions of the M-S plots near the flat-band potential (V_{fb}) where the depletion layer remains very thin was used to calculate the carrier density, according to the equation:

$$N_d = (2/e_0\varepsilon\varepsilon_0)[\mathrm{d}(1/C^2)/\mathrm{d}V]^{-1}$$

where e_0 is the electron charge, ε the dielectric constant of α-Fe_2O_3 (ε = 80)[11], ε_0 the permittivity of free space, N_d the donor density, and V the applied bias at the electrode. The electron densities of pristine α-Fe_2O_3 and Ag-doped α-Fe_2O_3 (Ag/Fe-0.05) nanorod films are calculated to be 2.6 × 10^{19} cm^{-3} and 1.2 × 10^{20} cm^{-3}, respectively. This 5-fold increase in the carrier density confirms the conjecture of increased carrier density of α-Fe_2O_3 upon Ag doping. It is well known that doping ions with higher valence states, such as Sn^{4+}, Ti^{4+} and Si^{4+}, *etc.*, can increase the electron concentration of α-Fe_2O_3, by acting as donor dopants. Here, Ag dopants could also act as electron donors with Ag^{I} turning to Ag^{III} *via* the charge transfer between Ag *5d* and O(*2p*)–Fe(*3d*) orbitals, as evidenced by the *in-situ* XANES spectra in the following section. The enhanced charge carrier density, which is linearly proportional to conductance according to the formula $\sigma = ne_0\mu_0$, leads to lower impedance for the Ag-doped samples. The enhanced electrical conductivity can extend the lifetime of charge carriers, giving rise to a reduction in the recombination of the electron–hole pairs[41]. Thus, the increased charge carrier density and reduced electron–hole recombination in the near-surface region by Ag surface doping is believed to be the major contributing factor for the pronounced photocurrent improvement of α-Fe_2O_3 nanorods in the present study. In addition, M–S analysis shows that the flat-band potential (V_{fb}) cathodically shifted by 74 mV when the Ag-doped overlayer was created on the surface of α-Fe_2O_3 nanorods by Ag^+ surface doping (Fig. 7). This flat-band potential shift is probably due to the efficient hole transport from the bulk α-Fe_2O_3 to the Ag-doped overlayer, accelerating the surface water oxidation reaction.

As generally accepted, α-Fe_2O_3 suffers from short hole diffusion length in the bulk and swift charge recombination on the surface, which greatly restricts the PEC efficiency of α-Fe_2O_3 as a photoanode[7]. Doping foreign metal ions such as Ti, Zr, and Sn into the bulk of α-Fe_2O_3 has proven to be an effective method of improving the conductivity and hence carrier migration ability of α-Fe_2O_3, contributing to increased PEC activity in the UV light region specifically[1,9,39,40]. To improve the utilization of low energy charge carriers and enhance the PEC energy conversion efficiency in the visible light region, it is important to avoid hole accumulation at the surface and inhibit surface charge recombination. Some metal oxides (IrO_2, Co_3O_4) or metal oxide mixtures (Fe-Ni oxide, Ni-Bi oxide) have been observed to significantly lower the overpotential for the water oxidation reaction by avoiding hole accumulation on the photoanode surface[10]. In our study, a thin $Ag_xFe_{2-x}O_3$ overlayer of ~2–3 nm was formed by Ag doping and evenly covered the α-Fe_2O_3 nanorod surface. Ag dopants effectively increase the charge carrier density in the near-surface region and lower the impendence for charge transfer, allowing more photoinduced holes in the near-surface region to transfer to the α-Fe_2O_3 nanorod surface. Additionally, as revealed by XANES analysis, higher extent of O(*2p*)–Fe(*3d*) hybridization induced by surface doping of Ag is believed to lead to increased oxygen electrocatalysis, which possibly renders the Ag-doped overlayer to act as water oxidation catalyst. Once arriving at the surface, as evidenced by XPS analysis (partial oxidation of Ag^{I} to Ag^{III} during initial period of PEC reaction), holes are captured by Ag^+ doping sites, which inhibits both surface hole accumulation and recombination of holes with either surface trapping sites or surface electrons, effectively promoting the water oxidiation process. Due to the increased carrier density by Ag doping and accelerated water oxidation reaction kinetics by the $Ag_xFe_{2-x}O_3$ overlayer, excited holes could quickly tranfer to the surface and participate in surface reactions with reduced bulk and surface recombination. As a result, the Ag-doped α-Fe_2O_3 nanorod films show greatly enhanced PEC performances relative to the pristine α-Fe_2O_3 nanorod film, which is more significant in the visible light region due to the more obvious acceleration effect of the $Ag_xFe_{2-x}O_3$ overlayer on the water oxidation reaction for low energy holes.

Without knowing the fundamental electronic structures of the material and how they operate upon its working condition, it is

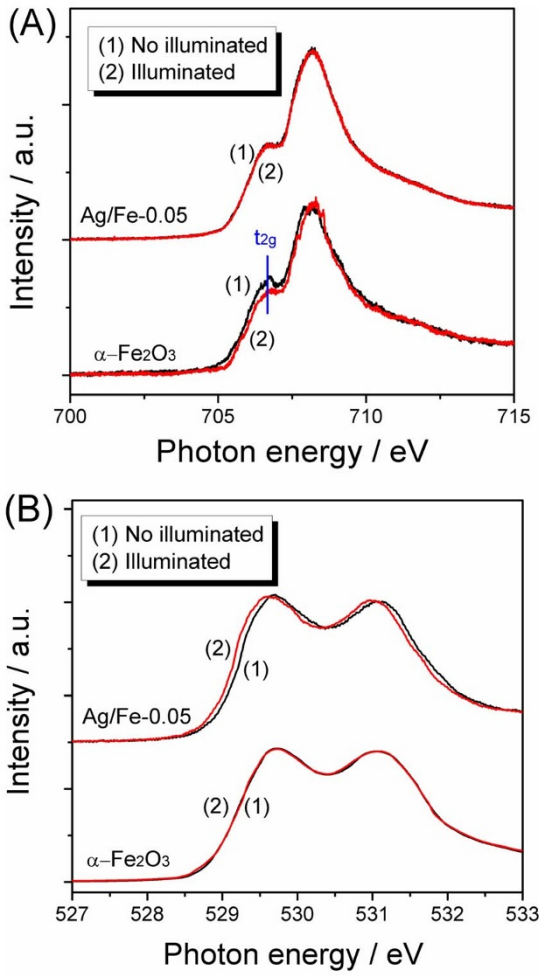

Figure 8 | ***In-situ*** **XANES spectra of (A) Fe *L*-edge and (B) O *K*-edge for the pristine and Ag-doped α-Fe_2O_3 (Ag/Fe-0.05) films recorded with and without illuminated condition.**

difficult to better understand and to better engineer the material for more practical use. Therefore, the *in-situ* XANES measurement of α-Fe_2O_3 and Ag-doped α-Fe_2O_3 nanorod films were conducted to further understand the possible mechanism of the water splitting reaction. The Fe *K*-, Fe $L_{2,3}$-, and O *K*-edge XANES spectra were recorded in the dark and illuminated condition by an 1.5 AM solar simulator.

Firstly, the *in-situ* Fe *K*-edge XANES spectra which probe the electron transition from 1*s* to 4*p* states are shown in Fig. S7. It is clear that no spectral differences can be observed for the pristine and Ag-doped α-Fe_2O_3 film with and without solar illumination, suggesting the hybridized Fe *3d* and O *2p* orbitals are active for the water splitting, rather than Fe *4p* orbitals.

The *in-situ* XANES spectra of Fe $L_{2,3}$-edge are presented in Fig. 8A. It is clear that no substantial spectral differences can be found in the Ag-doped α-Fe_2O_3 nanorod film with and without solar illumination, whereas a significant change in the Fe *3d* t_{2g} states is revealed for the pristine one. As the pristine α-Fe_2O_3 is exposed to the solar illumination, the intensity of Fe *3d* t_{2g} state is reduced compared with that without illumination. This indicates the Fe *3d* states are more critical in pristine α-Fe_2O_3 film than in Ag-doped one. Fig. 8B displays the *in-situ* O *K*-edge XANES spectra of α-Fe_2O_3 and Ag-doped α-Fe_2O_3 nanorod films with and without solar illumination. In contrast to the Fig. 8A, no subtle spectral change can be found in pristine α-Fe_2O_3 film but a remarkable spectral difference is revealed in the Ag-doped α-Fe_2O_3 film under the illuminated condition. Notably, the absorption edge is shifted to lower energy in illuminated condition than that without illumination. Besides, in the Ag-doped α-Fe_2O_3 film, the ratio of the intensity of the peak at around 529.6 eV to that around 531.0 eV declines in the illuminated condition. The observation of the spectral differences from Fig. 8A,B suggests that the mechanisms and the active orbitals in pristine and Ag-doped α-Fe_2O_3 film are different. The oxygen related hole is critical in Ag-doped α-Fe_2O_3 film and iron related hole dominates in the pristine one. These two different types of holes are consistent with a recent study that revealed two kinds of helpful holes (oxygen-related and iron-related holes) for water splitting[42].

The spectral change of the pristine α-Fe_2O_3 film upon the light irradiation may suggest that the electronic structure is only varied at the Fe *3d* orbital, implying the charge is probably accumulated at surface of nanorod and does not involve in the hybridized O(*2p*)−Fe(*3d*) orbitals. This implies that separation of electron-hole pair is not efficient in pristine α-Fe_2O_3, and it recombines easily at the surface. However, the remarkable spectral change of O *K*-edge of Ag-doped α-Fe_2O_3 film with and without solar illumination suggests the light-induced modification of conduction band. The conduction band is shifted to lower energy and may be beneficial for electron flow. The slight intensity decrease (increase) of the peak at around 529.6 eV (531.0 eV) in Ag-doped α-Fe_2O_3 film in the illuminated condition indicates the hybridized O(*2p*)−Fe($3d_{t2g}$) orbital gains some charges. The gain of the charges is believed to be related to the charge transfer between Ag *5d* and O(*2p*)−Fe(*3d*) orbitals, contributing to the increased charge carrier density with Ag dopants possibly acting as electron donors. The Ag may lose some charge in the initial stage, turning Ag^{I} to Ag^{III}, which has been illustrated by XPS analysis. Therefore, the possible mechanism of the $Ag_xFe_{2-x}O_3$ overlayer catalyzing the water oxidation reaction could be proposed

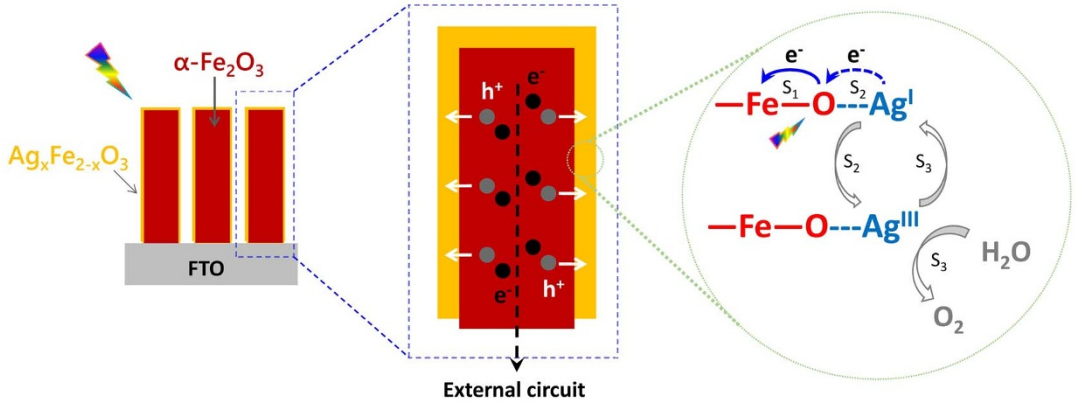

Figure 9 | **Core/shell structured α-Fe_2O_3/$Ag_xFe_{2-x}O_3$ nanorods and schematic of water oxidation reaction accelerated by $Ag_xFe_{2-x}O_3$ overlayer.**

in Fig. 9. Upon solar light irradiation, the electrons are excited from oxygen to iron (S_1), the oxygen-related holes then render Ag^I to be oxidized to Ag^{III} (S_2). The oxidized Ag^{III} species could promote water oxidation to produce oxygen, and meanwhile be reduced back to Ag^I (S_3). Such a multistep charge transfer process is supposed to prevent the recombination of oxygen-related holes with surface trapping sites or surface electrons and hence catalyzes the water oxidation reaction.

In summary, we have demonstrated a facile solution-based surface treatment method, through which a thin, Ag-doped overlayer of ~2–3 nm was evenly formed along the α-Fe_2O_3 nanorods. As a photoanode for light-induced water splitting, the obtained α-Fe_2O_3/$Ag_xFe_{2-x}O_3$ core/shell nanorod films demonstrated enhanced photoelectrochemical performance relative to the pristine α-Fe_2O_3 nanorod film, especially in the visible light region. IPCE at 400 nm was increased from 2.2% to 8.4% at 1.23 V vs. RHE. It is proposed that the carrier density was increased by Ag doping and the water oxidation reaction kinetics were accelerated by the $Ag_xFe_{2-x}O_3$ overlayer. Synergistically, these enhancements led to an increase in the photoelectrochemical performance of the α-Fe_2O_3/$Ag_xFe_{2-x}O_3$ core/shell nanorod film by reducing bulk and surface charge carrier recombination. This design of core/shell structured photoanodes from low cost hematite "rust" reveals potential applications for developing highly efficient water-splitting materials for solar hydrogen generation.

Methods

Fabrication of α-Fe_2O_3 nanorod arrays with Ag-doped overlayer. Step I: β-FeOOH nanorod arrays were grown on FTO glass in an aqueous solution as reported by Vayssieres[43], with minor modification. Typically, two back-to-back FTO substrates (Pilkington, TEC7) were put into a cap-sealed glass bottle containing an aqueous solution of 0.15 M ferric chloride ($FeCl_3 \cdot 6H_2O$), and 1 M sodium nitrate ($NaNO_3$), leaning against the wall of the glass bottle. The pH values of these aqueous solutions were set at 1.35. The glass bottles were then transferred into a regular oven and kept at 100°C for 24 h, before naturally cooled to room temperature. The obtained yellow films of β-FeOOH nanorod arrays were washed with distilled water and dried.

Step II: β-FeOOH nanorod films were immersed into 20 mL of aqueous solution of silver acetate (AgAc), and ultrasonicated for 10 min. The resultant Ag^+/β-FeOOH films were then rinsed with ethanol and dried in air.

Step III: The Ag^+/β-FeOOH films were transformed to $Ag_xFe_{2-x}O_3$/α-Fe_2O_3 by annealing at 750°C for 5 min, with a ramping rate of 25°C/min.

The obtained $Ag_xFe_{2-x}O_3$/α-Fe_2O_3 nanorod films were denoted as Ag/Fe-*n*, where $n = 0.005$, 0.01, 0.05, 0.1. Aqueous solutions of AgAc with different concentrations (0.005, 0.01, 0.05, and 0.1 M) were used in Step II.

Characterization. X-ray diffraction patterns (XRD) were obtained from a PANalytical X'pert MPD Pro diffractometer using Ni-filtered Cu Kα irradiation (wavelength 1.5406 Å) the voltage used was 40 kV and the current was 40 mA. Scanning electron microscopy (SEM) was taken on a JEOL 7800F SEM with an accelerating voltage of 15 kV. Raman scattering studies were performed on a Jobin Yvon LabRAM HR spectrometer using 514.5 nm irradiation from an argon ion laser at 20 mW. Spectral transmittance was measured on a HITACHI U4100 instrument equipped with a lab-sphere diffuse reflectance accessory. The X-ray photoelectron spectroscopy (XPS) measurements were conducted on a Kratos spectrometer (AXIS Ultra DLD) with monochromatic Al Kα radiation ($h\nu = 1486.69$ eV) and with a concentric hemispherical analyzer. Transmission electron microscopy (TEM) was carried out in an FEI Tecnai G2 F30 microscope working at 300 kV. The XANES at the O *K*-edge, and Fe *L*-edge were obtained on the Spherical Grating Monochromatorrocharac Beamline at the Canadian Light Source (CLS), a 2.9 GeV third generation synchrotron source, using a Si(111) double crystal monochromator and were recorded in the surface sensitive total electron yield (TEY). The *in-situ* XANES measurement of O *K*- and Fe $L_{2,3}$-edges, and Fe *K*-edge were carried out at BL20A1 and BL17C1, respectively, at National Synchrotron Radiation Research Center (NSRRC), Taiwan. O *K*-edge and Fe $L_{2,3}$-edges were collected with TEY and Fe *K*-edge was recorded with total fluorescence yield mode. The XANES spectra were taken in the dark (without illumination) and illumination by an 1.5 AM solar simulator (HAL-302, Asahi Spectra, Japan).

Photoelectrochemical measurement. Photoelectrochemical measurements were performed using a three-electrode configuration in 0.5 M NaCl (pH 6.7) aqueous solution at a potentiostat (Pine Instruments Bipotentiostat), with the pristine and Ag-doped α-Fe_2O_3 nanorod arrays as the working photoanodes, Ag/AgCl as the reference electrode, and Pt as the counter electrode. A 1 cm^2 masked-off, sealed area of photoanodes was irradiated with a 300 W Xe lamp solar simulator with adjustable power settings through an AM 1.5G filter (Oriel). The light intensity at the sample location in the photoelectrochemical cell was 100 $mW \cdot cm^{-2}$ as measured by a power detector (Newport). N_2 gas was continuously bubbled in solution before and during the experiment to remove any dissolved O_2 and therefore suppress the reduction of O_2 at the counter electrode.

IPCE measurements were performed using a 300 W Xe lamp integrated with a computer-controlled monochromator (Beijing Optic Instrument Factory), a photochopper (PARC), and a lock-in amplifier (Signal Recovery) for photocurrent detection. The absolute intensity of the incident light from the monochromator was measured with a radiometer/photometer (International Light). All IPCE measurements were carried out under potential-controlled conditions, with 0.65 V as applied potential versus Ag/AgCl reference electrode (i.e., 1.23 V versus reversible hydrogen electrode (RHE), calculated from $E_{RHE} = E_{Ag/AgCl} + 0.1976 + 0.057 \cdot pH$). Mott–Schottky measurements in the dark were performed in a 0.5 M Na_2SO_4 electrolyte with the same three-electrode configuration.

1. Shen, S. Towards efficient solar water splitting over hematite photoelectrodes. *J. Mater. Res.* **29**, 29–46 (2014).
2. Sivula, K., Formal, F. L. & Grätzel, M. Solar water splitting: Progress using hematite (α-Fe_2O_3) photoelectrodes. *ChemSusChem* **4**, 432–449 (2011).
3. Katz, M. J. *et al.* Toward solar fuels: Water splitting with sunlight and "rust"? *Coordin. Chem. Rev.* **256**, 2521–2529 (2012).
4. Mayer, M. T., Lin, Y., Yuan, G. & Wang, D. Forming heterojunctions at the nanoscale for improved photoelectrochemical water splitting by semiconductor materials: Case studies on hematite. *Acc. Chem. Res.* **46**, 1558–1566 (2013).
5. Kennedy, J. H. & Frese, J. K. W. Photooxidation of water at alpha-Fe_2O_3 electrodes. *J. Electrochem. Soc.* **125**, 709–714 (1978).
6. Morin, F. J. Electrical Properties of α-Fe_2O_3. *Phys. Rev.* **93**, 1195–1199 (1954).
7. Wheeler, D. A., Wang, G., Ling, Y., Li, Y. &Zhang, J. Z. Nanostructured hematite: Synthesis, characterization, charge carrier dynamics, and photoelectrochemical properties. *Energy Environ. Sci.* **5**, 6682–6702 (2012).
8. Wang, G. *et al.* Facile synthesis of highly photoactive α-Fe_2O_3-based films for water oxidation. *Nano Lett.* **11**, 3503–3509 (2011).
9. Shen, S. *et al.* Physical and photoelectrochemical properties of Zr-doped hematite nanorod arrays. *Nanoscale* **5**, 9867–9874 (2013).
10. Shen, S. & Mao, S. S. Nanostructure designs for effective solar-to-hydrogen conversion. *Nanophotonic* **1**, 31–50 (2012).
11. Formal, F. L. *et al.* Passivating surface states on water splitting hematite photoanodes with alumina overlayers. *Chem. Sci.* **2**, 737–743 (2011).
12. Barroso, M. *et al.* Dynamics of photogenerated holes in surface modified α-Fe_2O_3 photoanodes for solar water splitting. *PNAS* **109**, 15640–15645 (2012).
13. Xi, L. *et al.* Surface treatment of hematite photoanodes with zinc acetate for water oxidation. *Nanoscale* **4**, 4430–4433 (2012).
14. Tilley, S. D., Cornuz, M., Sivula, K. & Grätzel, M. Light-induced water splitting with hematite: Improved nanostructure and iridium oxide catalysis. *Angew. Chem. Int. Ed.* **49**, 6405–6408 (2010).
15. Riha, S. C. *et al.* Atomic layer deposition of a sub-monolayer catalyst for the enhanced photoelectrochemical performance of water oxidation with hematite. *ACS Nano* **7**, 2396–2405 (2013).
16. Zhong, D. K., Sun, J., Inumaru, H. & Gamelin, D. R. Solar water oxidation by composite catalyst/α-Fe_2O_3 photoanodes. *J. Am. Chem. Soc.* **131**, 6086–6087 (2009).
17. Wang, G. *et al.* A mechanistic study into the catalytic effect of $Ni(OH)_2$ on hematite for photoelectrochemical water oxidation. *Nanoscale* **5**, 4129–4133 (2013).
18. Kim, J. Y. *et al.* Single-crystalline, wormlike hematite photoanodes for efficient water splitting. *Sci. Rep.* **3**, 2681 (2013).
19. Shen, S., Kronawitter, C. X., Jiang, J., Mao, S. S. & Guo, L. Surface tuning for promoted charge transfer in hematite nanorod arrays as water-splitting photoanodes. *Nano Res.* **5**, 327–336 (2012).
20. Shen, S. *et al.* Effect of Cr doping on the photoelectrochemical performance of hematite nanorod photoanodes. *Nano Energy* **1**, 732–741 (2012).
21. Spray, R. L., McDonald, K. J. & Choi, K.-S. Enhancing photoresponse of nanoparticulate α-Fe_2O_3 electrodes by surface composition tuning. *J. Phys. Chem. C* **115**, 3497–3506 (2011).
22. Franking, R. *et al.* Facile post-growth doping of nanostructured hematite photoanodes for enhanced photoelectrochemical water oxidation. *Energy Environ. Sci.* **6**, 500–512 (2013).
23. Xi, L. *et al.* A novel strategy for surface treatment on hematite photoanode for efficient water oxidation. *Chem. Sci.* **4**, 164–169 (2013).
24. Cheng, W. *et al.* Ni-doped overlayer hematite nanotube: A highly photoactive architecture for utilization of visible light. *J. Phys. Chem. C* **116**, 24060–24067 (2012).
25. Vayssieres, L. On the design of advanced metal oxide nanomaterials. *Int. J. Nanotechnol.* **1**, 1–41 (2004).
26. Schön, G. ESCA studies of Ag, Ag_2O and AgO. *Acta Chem. Scand.* **27**, 2623–2633 (1973).
27. Li, L. *et al.* Facile solution synthesis of α-$FeF_3 \cdot 3H_2O$ nanowires and their conversion to α-Fe_2O_3 nanowires for photoelectrochemical application. *Nano Lett.* **12**, 724–731 (2012).
28. Morrish, R., Rahman, M., MacElroy, D. J. M. & Wolden, C. A. Activation of hematite nanorod arrays for photoelectrochemical water splitting. *ChemSusChem* **4**, 474–479 (2011).

29. Deng, J. *et al.* Ti-doped hematite nanostructures for solar water splitting with high efficiency. *J. Appl. Phys.* **112**, 084312 (2012).
30. Shen, S., Jiang, J., Guo, P. & Guo, L. Facile growth of porous hematite films for photoelectrochemical water splitting. *Int. J. Photoenergy* **2013**, 174982 (2013).
31. Wang, J., Zhou, J., Hu, Y. & Regier, T. Chemical interaction and imaging of single Co_3O_4/graphene sheets studied by scanning transmission X-ray microscopy and X-ray absorption spectroscopy. *Energy Environ. Sci.* **6**, 926–934 (2013).
32. Kronawitter, C. X. *et al.* TiO_2-SnO_2:F interfacial electronic structure investigated by soft x-ray absorption spectroscopy. *Phys. Rev. B* **85**, 125109 (2012).
33. Pollak, M. *et al.* An in-situ study of the surface phase transitions of α-Fe_2O_3 by X-ray absorption spectroscopy at the oxygen K edge. *Nucl. Instr. Meth. Phys. Res. Sec. B* **97**, 383–386 (1995).
34. Zhou, J. *et al.* Spectroscopic understanding of ultra-high rate performance for $LiMn_{0.75}Fe_{0.25}PO_4$ nanorods-graphene hybrid in lithium ion battery. *Phys. Chem. Chem. Phys.* **14**, 9578–9581 (2012).
35. Kronawitter, C. X. *et al.* Electron enrichment in 3d transition metal oxide hetero-nanostructures. *Nano Lett.* **11**, 3855–3861 (2011).
36. de Groot, F. M. F. *et al.* Oxygen 1s X-ray-absorption edges of transition-metal oxides. *Phys. Rev. B* **40**, 5715–5723 (1989).
37. Suntivich, J. *et al.* Estimating hybridization of transition metal and oxygen states in perovskites from O K-edge X-ray absorption spectroscopy. *J. Phys. Chem. C* **118**, 1856–1863 (2014).
38. Chen, J. G. NEXAFS investigations of transition metal oxides, nitrides, carbides, sulfides and other interstitial compounds. *Surf. Sci. Rep.* **30**, 1–152 (1997).
39. Shen, S. *et al.* Physical and photoelectrochemical characterization of Ti-doped hematite photoanodes prepared by solution growth. *J. Mater. Chem. A* **1**, 14498–14506 (2013).
40. Ling, Y., Wang, G., Wheeler, D. A., Zhang, J. Z. & Li, Y. Sn-doped hematite nanostructures for photoelectrochemical water splitting. *Nano Lett.* **11**, 2119–2125 (2011).
41. Meng, X. Y. *et al. Appl. Phys. Lett.* **98**, 112104 (2011).
42. Braun, A. *et al.* Direct observation of two electron holes in a hematite photoanode during photoelectrochemical water splitting. *J. Phys. Chem. C* **116**, 16870–16875 (2012).
43. Vayssieres, L., Beermann, N., Lindquist, S.-E. & Hagfeldt, A. Controlled aqueous chemical growth of oriented three-dimensional crystalline nanorod arrays: Application to iron(III) oxides. *Chem. Mater.* **13**, 233–235 (2001).

Acknowledgments

The authors gratefully acknowledge the financial support of the National Natural Science Foundation of China (Nos. 51102194, 51323011, 51121092), the Natural Science Foundation of Shaanxi Province (No. 2014KW07-02), the Natural Science Foundation of Jiangsu Province (No. BK20141212) and the Nano Research Program of Suzhou City (No. ZXG201442, No. ZXG2013003). S. Shen is supported by the Foundation for the Author of National Excellent Doctoral Dissertation of P. R. China (No. 201335) and the "Fundamental Research Funds for the Central Universities". The authors also would like to thank Canadian Light Source Inc. for support with the XAS measurement, and thank Prof. J. Z. Zhang and Ms. S. A. Lindley at UC Santa Cruz for their suggestive comments.

Author contributions

L.G. and S.S.M. planned the project. S.S. managed and performed the detailed experiments and wrote the paper, J.Z. and Y.H. conducted the XANES experiments. C.L.D. and E.N.T. conducted the in-situ XANES experiments. P.G. conducted the XPS measurements. All the authors discussed the results and commented on the manuscript.

Additional information

Supplementary information accompanies this paper at http://www.nature.com/scientificreports

Competing financial interests: The authors declare no competing financial interests.

How to cite this article: Shen, S. *et al.* Surface Engineered Doping of Hematite Nanorod Arrays for Improved Photoelectrochemical Water Splitting. *Sci. Rep.* **4**, 6627; DOI:10.1038/srep06627 (2014).